

Error Calculation of Large-Amplitude Internal Solitary Waves Within the Pycnocline Introduced by the Strong Stratification Approximation

Cunguo Xu¹, Zhan Wang^{1,2,3} and Hayatdavoodi Masoud^{2,4}

Received: 03 October 2022 / Accepted: 17 November 2022
© Harbin Engineering University and Springer-Verlag GmbH Germany, part of Springer Nature 2023

Abstract

At present, studies on large-amplitude internal solitary waves mostly adopt strong stratification models, such as the two- and three-layer Miyata–Choi–Camassa (MCC) internal wave models, which omit the pycnocline or treat it as another fluid layer with a constant density. Because the pycnocline exists in real oceans and cannot be omitted sometimes, the computational error of a large-amplitude internal solitary wave within the pycnocline introduced by the strong stratification approximation is unclear. In this study, the two- and three-layer MCC internal wave models are used to calculate the wave profile and wave speed of large-amplitude internal solitary waves. By comparing these results with the results provided by the Dubreil–Jacotin–Long (DJL) equation, which accurately describes large-amplitude internal solitary waves in a continuous density stratification, the computational errors of large-amplitude internal solitary waves at different pycnocline depths introduced by the strong stratification approximation are assessed. Although the pycnocline thicknesses are relatively large (accounting for 8%–10% of the total water depth), the error is much smaller under the three-layer approximation than under the two-layer approximation.

Keywords Internal solitary wave; Pycnocline; Two-layer approximation; Three-layer approximation; MCC internal wave model; DJL equation; Wave profile; Wave speed

Article Highlights

- The two- and three-layer MCC internal wave models and the DJL equation are used to study large-amplitude internal solitary waves.
- The error on profiles and speed of the internal solitary waves introduced by the strong stratification approximation are obtained.
- Three pycnocline thicknesses are considered to study the error of strong stratification approximation on describing internal solitary waves.

✉ Zhan Wang
zhan.wang@hrbeu.edu.cn

¹ Qingdao Innovation and Development Center of Harbin Engineering University, Qingdao 266555, China

² College of Shipbuilding Engineering, Harbin Engineering University, Harbin 150001, China

³ Frontiers Science Center for Wave Field of Extreme Ocean Environment, Harbin Engineering University, Harbin 150001, China

⁴ Civil Engineering Department, School of Science and Engineering, University of Dundee, Dundee DD1 4HN, UK

1 Introduction

Internal waves always exist in density-stratified oceans. The South China Sea is an area of frequent large-amplitude internal waves. Huang et al. (2016) observed a large-amplitude internal solitary wave with an amplitude of 240 m in the South China Sea. Large-amplitude internal solitary waves pose a great threat to the safety of underwater structures. For example, the KRI Nanggala-402 submarine crashed during an exercise in 2021, causing the deaths of 53 sailors (Gong et al. 2022). The main reason for the crash is believed to be that the submarine encountered large internal waves. Therefore, great importance is associated with accurately describing the characteristics of large-amplitude internal waves.

For the internal wave problem, most studies neglect the thickness of the pycnocline and approximate it to a two-layer fluid problem. The two-layer Miyata–Choi–Camassa (MCC) (Miyata 1985, 1988; Choi and Camassa 1999) internal wave model is widely used to study large-amplitude internal solitary waves. In the two-layer MCC model, only the depth-averaged horizontal velocity of the particles in

each layer is considered. Many studies have shown that the two-layer MCC model can accurately describe the large-amplitude internal waves in a two-layer fluid system for shallow configurations ($h_1/\lambda \ll 1$ and $h_2/\lambda \ll 1$, where h_1 and h_2 are the undisturbed thicknesses of the upper- and lower-fluid layers, respectively, and λ is the characteristic wavelength of the internal wave) (Choi and Camassa 1999; Camassa et al. 2006; Xie et al. 2010; Gao et al. 2012; Huang et al. 2013; la Forgia and Sciortino 2019; Du et al. 2019; Zou et al. 2020; Cui et al. 2021).

Compared with the two-layer strong stratification approximation, a more suitable approach is to approximate the practical fluid system as a three-layer fluid system where the pycnocline is treated as another fluid layer with a constant density (Jo and Choi 2014). Barros et al. (2020) derived a three-layer internal wave model in which a depth-averaged horizontal velocity is introduced for each layer. This model can be considered a generalized two-layer MCC model, i.e., a three-layer MCC model. Zhang et al. (2020) demonstrated that the three-layer MCC internal wave model can accurately describe the large-amplitude internal solitary waves in a three-layer fluid system for shallow configurations ($h_1/\lambda \ll 1$, $h_2/\lambda \ll 1$, and $h_3/\lambda \ll 1$, where h_1 , h_2 , and h_3 are the undisturbed thicknesses of the upper-, middle-, and lower-fluid layers, respectively, and λ is the characteristic wavelength of the internal wave) by comparing with laboratory measurements.

When the pycnocline thickness is small or negligible, the two- and three-layer internal wave models can accurately describe large-amplitude internal waves (Grue et al. 1999; Huang et al. 2013; la Forgia and Sciortino 2021). However, pycnocline thickness in real oceans cannot be ignored sometimes. Under such conditions, using the strong stratification approximation to calculate large-amplitude internal solitary waves will introduce certain errors. Cheng and Hsu (2014) and Lu et al. (2021) noted that the internal wave speed decreases with increasing pycnocline thickness. Nevertheless, the computational error of a large-amplitude internal wave within the pycnocline introduced by the strong stratification approximation should be further studied.

In this paper, we apply the two- and three-layer MCC internal wave models to calculate the wave profile and wave speed of large-amplitude internal solitary waves. Meanwhile, we also use the open-source solver (Dunphy et al. 2011) to obtain the results of the Dubreil–Jacotin–Long (DJL) equation (Dubreil–Jacotin 1934; Long 1953), given that this equation is formally equivalent to the full set of Euler equations that can accurately describe the large-amplitude mode-1 internal solitary waves in continuous density stratification when the environment is unchanging (Stastna and Lamb 2002; Dunphy et al. 2011; Stastna and Lamb 2020). Through comparison, the errors introduced by the strong stratification approximation under different pycnocline thicknesses are obtained.

2 Theoretical models

In this section, we will briefly introduce the theoretical models that are applied in this paper for describing large-amplitude internal waves.

2.1 Two-layer MCC internal wave model

Figure 1 shows a sketch of an internal solitary wave in a two-layer fluid system.

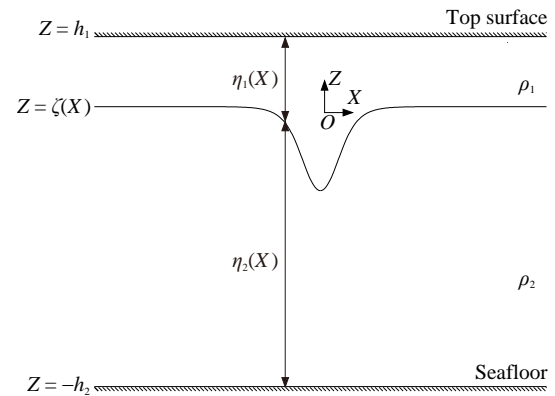


Figure 1 Internal solitary wave in a two-layer fluid system

The fluids are assumed to be inviscid, incompressible, and immiscible. The density and undisturbed thickness of each layer are ρ_i and h_i , respectively, where the subscripts $i = 1$ and $i = 2$ represent the variables for the upper- and lower-fluid layers, respectively. A wave-coordinate system OXZ , which travels with the internal wave at the same speed c , is established. The OX -axis is set at the undisturbed interface and positive to the right, and OZ is positive up. The internal solitary wave crest is set at $X = 0$. The upper surface of the upper-fluid layer, the interface between the two-fluid layers, and the lower surface of the lower-fluid layer are expressed as $Z = h_1$, $Z = \zeta(X)$, and $Z = -h_2$, respectively. The local thicknesses of the upper- and lower-fluid layers are expressed as $\eta_1(X)$ and $\eta_2(X)$, respectively.

In the two-layer MCC internal wave model, for a given internal wave amplitude a , the internal wave speed c can be obtained as

$$c = \sqrt{\frac{(h_1 - a)(h_2 + a)}{h_1 h_2 - (c_0^2 - g)a}} c_0 \quad (1)$$

where g is the acceleration of gravity, and c_0 is the linear long wave speed, given by

$$c_0 = \sqrt{\frac{gh_1 h_2 (\rho_2 - \rho_1)}{\rho_1 h_2 + \rho_2 h_1}} \quad (2)$$

Then, the wave profile can be obtained by solving the following equation:

$$(\zeta_x)^2 - \frac{3\zeta^2[\rho_1 c^2 \eta_2 + \rho_2 c^2 \eta_1 - g(\rho_2 - \rho_1)\eta_1 \eta_2]}{\rho_1 c^2 h_1^2 \eta_2 + \rho_2 c^2 h_2^2 \eta_1} = 0 \quad (3)$$

where

$$\eta_1 = h_1 - \zeta \quad (4)$$

$$\eta_2 = h_2 + \zeta \quad (5)$$

A detailed derivation of the two-layer MCC internal wave model and the related numerical algorithm is provided by Choi and Camassa (1999).

2.2 Three-layer MCC internal wave model

Figure 2 shows a sketch of an internal solitary wave in a three-layer fluid system.

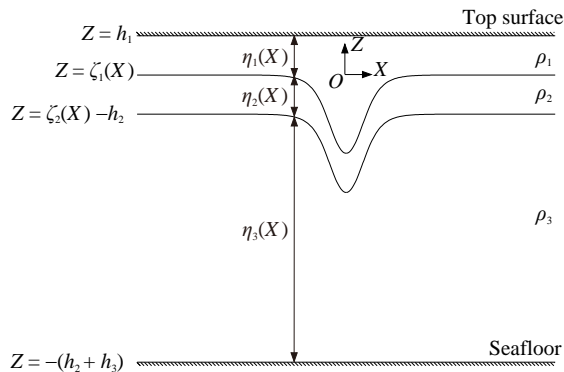


Figure 2 Internal solitary wave in a three-layer fluid system

The assumptions of the fluid layers and the establishment of the coordinate axes are similar to those in Section 2.1. The upper surface of the upper-fluid layer, the interface between the upper- and middle-fluid layers, the interface between the middle- and lower-fluid layers, and the lower surface of the lower-fluid layer are expressed as $Z = h_1$, $Z = \zeta_1(X)$, $Z = \zeta_2(X) - h_2$, and $Z = -(h_2 + h_3)$, respectively. The local thicknesses of the upper-, middle-, and lower-fluid layers are expressed as $\eta_1(X)$, $\eta_2(X)$, and $\eta_3(X)$, respectively.

In the three-layer MCC internal wave model, the wave profile and wave speed can be obtained by solving the following equations (Barros et al. 2020):

$$c^2 \left\{ \frac{1}{3} \left(\frac{h_1^2}{\eta_1} + \frac{h_2^2}{\eta_2} \right) \zeta_{1xx} + \frac{1}{6} \frac{h_2^2}{\eta_2} \zeta_{2xx} + \frac{1}{6} \left(\frac{h_1^2}{\eta_1^2} - \frac{h_2^2}{\eta_2^2} \right) \zeta_{1x}^2 + \frac{1}{3} \frac{h_2^2}{\eta_2^2} \zeta_{1x} \zeta_{2x} + \frac{1}{3} \frac{h_2^2}{\eta_2^2} \zeta_{2x}^2 \right\} = \frac{1}{2} c^2 \left(\frac{h_1^2}{\eta_1^2} - \frac{h_2^2}{\eta_2^2} \right) - g \left(1 - \frac{\rho_1}{\rho_2} \right) \zeta_1 \quad (6)$$

$$c^2 \left\{ \frac{1}{6} \frac{h_2^2}{\eta_2} \zeta_{1xx} + \frac{1}{3} \left(\frac{h_2^2}{\eta_2} + \frac{h_3^2}{\eta_3} \right) \zeta_{2xx} - \frac{1}{3} \frac{h_2^2}{\eta_2^2} \zeta_{1x}^2 - \frac{1}{3} \frac{h_2^2}{\eta_2^2} \zeta_{1x} \zeta_{2x} + \frac{1}{6} \left(\frac{h_2^2}{\eta_2^2} - \frac{h_3^2}{\eta_3^2} \right) \zeta_{2x}^2 \right\} = \frac{1}{2} c^2 \left(\frac{h_2^2}{\eta_2^2} - \frac{h_3^2}{\eta_3^2} \right) - g \left(\frac{\rho_3}{\rho_2} - 1 \right) \zeta_2 \quad (7)$$

where

$$\eta_1 = h_1 - \zeta_1 \quad (8)$$

$$\eta_2 = \zeta_1 - \zeta_2 + h_2 \quad (9)$$

$$\eta_3 = h_3 + \zeta_2 \quad (10)$$

For a detailed derivation of the three-layer MCC internal wave model, we refer the reader to Barros et al. (2020). The numerical algorithm used for the steady-state solution of the three-layer internal wave model is given in Wang (2021).

2.3 DJL equation

The DJL equation describes steady large-amplitude internal solitary waves in a continuously stratified fluid. The density profile of the fluid is described by $\rho(Z) = \rho_0 + \rho_r(Z)$, where ρ_0 is the reference density. Under the Boussinesq and rigid-lid assumptions, the DJL equation is written as (Dubreil-Jacotin 1934; Long 1953):

$$\nabla^2 \zeta + \frac{N^2(Z - \zeta)}{c^2} \zeta = 0 \quad (11)$$

where $\zeta(X, Z)$ represents the isopycnic displacement (internal wave elevation),

$$N(Z) = \sqrt{-\frac{g}{\rho_0} \frac{d\rho_r}{dZ}} \quad (12)$$

is the buoyancy frequency, and c is the speed of the internal solitary wave, which is obtained together with $\zeta(X, Z)$.

For a detailed derivation of the DJL equation, we refer the reader to Dubreil-Jacotin (1934) and Long (1953). A detailed solution algorithm and the solution to the DJL equation are given by Dunphy et al. (2011).

In this paper, we focus on the steady solutions of internal solitary waves in a flat bottom (i.e., the internal solitary waves propagate through an unchanging environment), which can be accurately described by the DJL equation (Stastna and Lamb 2020). Hence, the results provided by the DJL equation are treated as the benchmark solutions.

3 Numerical test cases

In this section, we consider the wave profile and wave

speed of large-amplitude internal solitary waves under three types of pycnoclines. The results of the two- and three-layer MCC internal wave models are compared with the results of the DJL equation, and the errors introduced by the strong stratification approximation are obtained. Relevant case parameters are shown in Table 1. We note that Case A, Case B, and Case C belong to shallow configurations and apply to the MCC internal wave model. H and d represent the total water depth and the pycnocline thickness, respectively. The parameters of Case A are selected from the physical experiments conducted by Grue et al. (1999). The parameters of Case B and Case C are selected from the measurements in real oceans by Kuang (1986).

3.1 Description of the pycnocline

In this paper, the pycnocline is described as (Camassa and Tiron 2011):

$$\rho(Z) = \rho_{\min} + \frac{\rho_{\max} - \rho_{\min}}{2} \left\{ 1 + \tanh \left[\alpha (Z_p - Z) \right] \right\} \quad (13)$$

where ρ_{\min} and ρ_{\max} are the minimum and maximum values of the density, respectively, and Z_p is the vertical position of the center of the pycnocline. α is a parameter related to the pycnocline thickness. By defining the upper and lower boundaries of the pycnocline corresponding to the vertical positions where the density is $\rho_{\min} + 0.1(\rho_{\max} - \rho_{\min})$ and $\rho_{\max} - 0.1(\rho_{\max} - \rho_{\min})$, respectively, the pycnocline thickness can be obtained, and the value of α can be further determined.

Figure 3 shows the pycnocline profiles for Cases A, B, and C, where we have translated the vertical position of the pycnocline center $Z_p - Z = 0$.

3.2 Results and discussions

We use the two- and three-layer MCC internal wave models and the DJL equation to calculate the profile and speed of large-amplitude internal solitary waves for Cases A, B, and C. For the two-layer MCC internal wave model, the internal wave profile to be compared with is $\zeta(X)$, presented in Section 2.1; for the three-layer MCC internal wave model, $(\zeta_1(X) + \zeta_2(X))/2$, presented in Section 2.2; for the DJL equation, the isopycnic displacement for the

density $(\rho_{\max} - \rho_{\min})/2$.

3.2.1 Case A ($d/H = 3\%$)

The wave profiles of the two- and three-layer MCC internal wave models and the DJL equation are compared in Figure 4. The experimental results of Grue et al. (1999) are also included in this figure. We find that the three numerical results agree well with the experimental results.

The results of the internal solitary wave speed of the two amplitudes are shown in Table 2. Considering the results of the DJL equation as the benchmark solution, the results of the two- and three-layer MCC internal wave models are found to be very close to the results of the DJL equation, and the relative errors are within 2%.

It is observed that when the pycnocline thickness is small ($d/H = 3\%$), the relative error introduced by the strong stratification approximation for calculating the wave profile and wave speed is also very small.

3.2.2 Case B ($d/H = 8\%$)

The wave profiles of the two- and three-layer MCC internal wave models and the DJL equation are compared in Figure 5. Since experimental results are unavailable for comparison, we select the DJL results as the benchmark solution. From Figure 5, we find that the wave profile obtained by the two-layer MCC internal wave model is slightly wider, while the wave profiles obtained by the three-layer MCC internal wave model and the DJL equation agree well with each other.

To further investigate the difference between results, we consider the half-profile width $\lambda_{1/2}$, which is defined by Koop and Butler (1981) as the distance between the horizontal position of the peak and the horizontal position at half-wave amplitude. We set the results of the DJL equation as the benchmark values. Table 3 shows the results of this comparison.

We find that the relative errors introduced by the two- and three-layer MCC internal wave models are approximately 10% and within 2%, respectively.

The internal solitary wave speeds of the two amplitudes are shown in Table 4. The relative error is less than 4% and 2% between the two- and three-layer MCC internal wave models, respectively, and the DJL equation.

From these results, it is concluded that when the ratio of

Table 1 Parameters of the test cases considered in this study

Case	Two-layer		Three-layer		Continuous		Amplitude (m)	d/H (%)
	Density (kg/m ³)	Thickness (m)	Density (kg/m ³)	Thickness (m)	Density (kg/m ³)	Thickness (m)		
	ρ_1, ρ_2	h_1, h_2	ρ_1, ρ_2, ρ_3	h_1, h_2, h_3	ρ_{\min}, ρ_{\max}	H		
Case A	999:1 022	0.15:0.62	999:1 010.5:1 022	0.14:0.02:0.61	999–1022	0.77	0.136 5 0.184 5	3
Case B	1 025:1 028	125:525	1 025:1 026.5:1 028	100:50:500	1 025–1 028	650	120 160	8
Case C	1 025:1 028	16.6:83.4	1 025:1 026.5:1 028	11.4:10.4:78.2	1 025–1 028	100	15 20	10

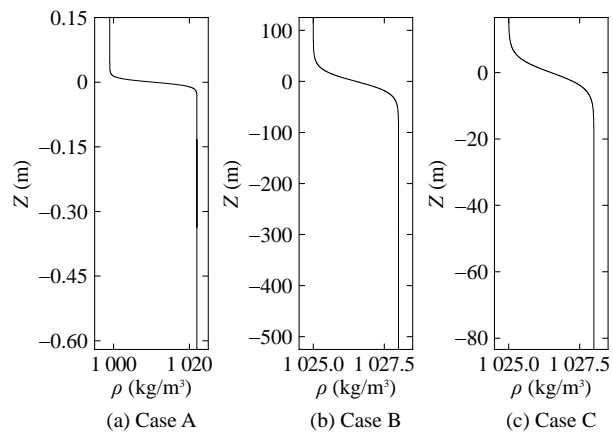


Figure 3 Density profiles of the three cases considered in this study

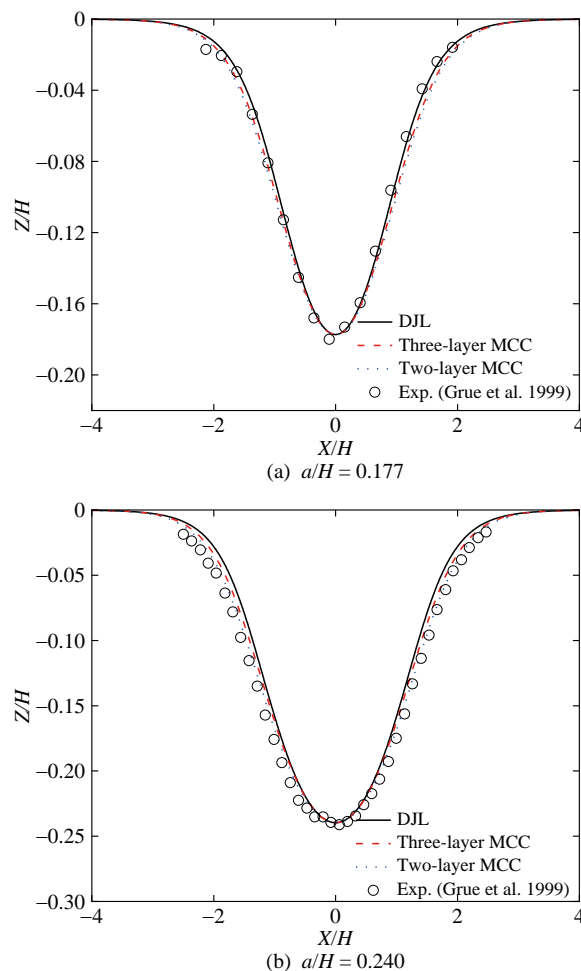


Figure 4 Comparison of the internal solitary wave profiles obtained by different models and laboratory measurements for Case A ($d/H = 3\%$)

the pycnocline thickness to the total water depth increases ($d/H = 8\%$), using the two-layer strong stratification approximation will introduce certain errors. Meanwhile, using the three-layer strong stratification approximation to calculate the wave profile and wave speed of large internal solitary waves does not introduce significant errors.

Table 2 Internal solitary wave speeds for Case A ($d/H = 3\%$)

Model	$a/H = 0.177$		$a/H = 0.240$	
	Speed $c/(gH)^{1/2}$	Relative error (%)	Speed $c/(gH)^{1/2}$	Relative error (%)
DJL	7.20×10^{-2}	—	7.42×10^{-2}	—
Two-layer MCC	7.31×10^{-2}	+1.53	7.50×10^{-2}	+1.08
Three-layer MCC	7.20×10^{-2}	0	7.39×10^{-2}	-0.40

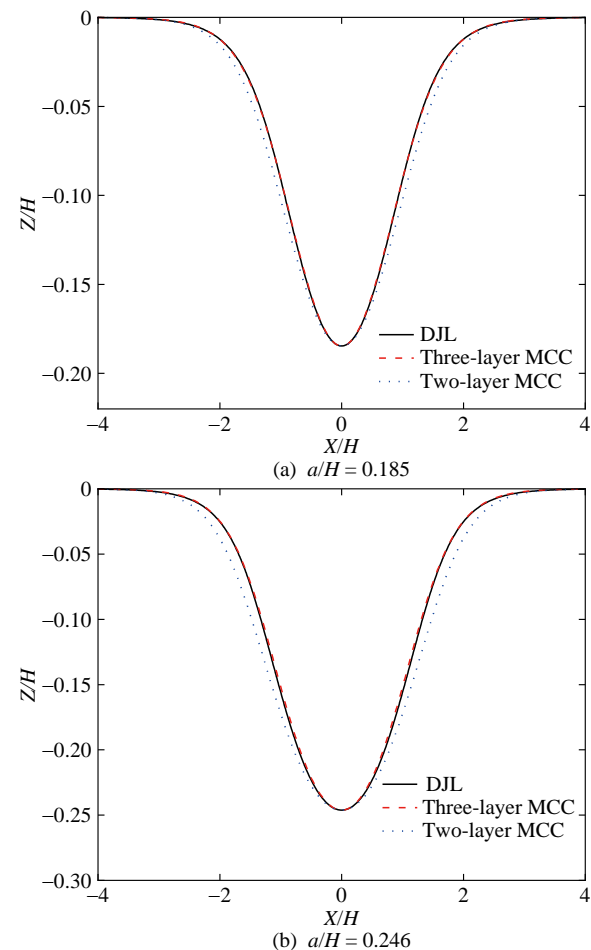


Figure 5 Comparison of the internal solitary wave profiles for Case B ($d/H = 8\%$)

Table 3 Internal solitary wave half-profile widths for Case B ($d/H = 8\%$)

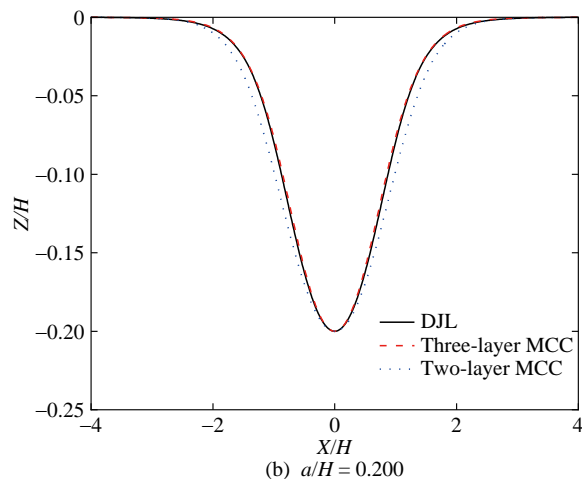
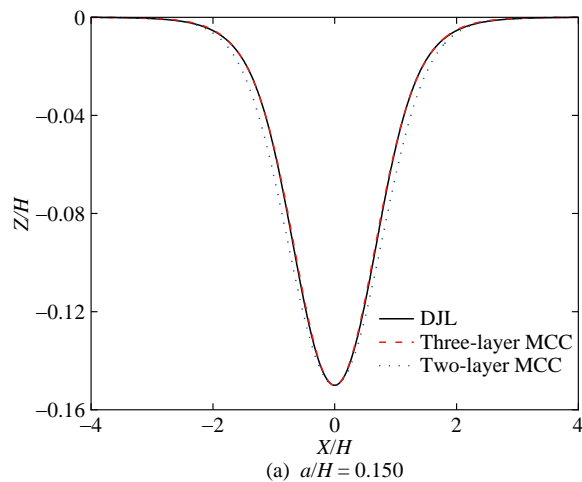
Model	$a/H = 0.185$		$a/H = 0.246$	
	Half profile $\lambda_{1/2}/H$	Relative error (%)	Half profile $\lambda_{1/2}/H$	Relative error (%)
DJL	0.991	—	1.191	—
Two-layer MCC	1.079	+8.88	1.326	+11.34
Three-layer MCC	0.989	-0.20	1.168	-1.93

3.2.3 Case C ($d/H = 10\%$)

The results of the two- and three-layer MCC internal wave models and the DJL equation are shown in Figure 6.

Table 4 Internal solitary wave speeds for Case B ($d/H = 8\%$)

Model	$a/H = 0.185$		$a/H = 0.246$	
	Speed $c/(gH)^{1/2}$	Relative error (%)	Speed $c/(gH)^{1/2}$	Relative error (%)
DJL	2.53×10^{-2}	–	2.6×10^{-2}	–
Two-layer MCC	2.62×10^{-2}	+3.56	2.68×10^{-2}	+3.08
Three-layer MCC	2.50×10^{-2}	–1.19	2.58×10^{-2}	–0.77

**Figure 6** Comparison of the internal solitary wave profiles for Case C ($d/H = 10\%$)

We observe that the wave profiles are obviously wider when obtained by the two-layer MCC internal wave model and generally consistent with the DJL equation when obtained by the three-layer MCC internal wave model.

The half-profile widths are compared in Table 5. The introduced relative errors of the two- and three-layer MCC internal wave models are approximately 12% and approximately 2%, respectively.

The internal solitary wave speeds of the two amplitudes are shown in Table 6. We find that the relative error between the two- and three-layer internal wave models and

Table 5 Internal solitary wave profiles for Case C ($d/H = 10\%$)

Model	$a/H = 0.150$		$a/H = 0.200$	
	Half profile $\lambda_{1/2}/H$	Relative error (%)	Half profile $\lambda_{1/2}/H$	Relative error (%)
DJL	0.816	–	0.875	–
Two-layer MCC	0.909	+11.40	0.986	+12.69
Three-layer MCC	0.806	–1.23	0.853	–2.51

the DJL equation reaches 6% and less than only 1%, respectively.

Table 6 Internal solitary wave speeds for Case C ($d/H = 10\%$)

Model	$a/H = 0.150$		$a/H = 0.200$	
	Speed $c/(gH)^{1/2}$	Relative error (%)	Speed $c/(gH)^{1/2}$	Relative error (%)
DJL	2.36×10^{-2}	–	2.46×10^{-2}	–
two-layer MCC	2.51×10^{-2}	+6.36	2.61×10^{-2}	+6.10
three-layer MCC	2.34×10^{-2}	–0.85	2.44×10^{-2}	–0.81

Hence, when the ratio of pycnocline thickness to the total water depth further increases ($d/H = 10\%$), calculating the wave profile and wave speed of large internal solitary waves will lead to significant errors when the two-layer strong stratification approximation is used but can be effectively accomplished using the three-layer strong stratification approximation.

4 Conclusions

To study the influence of the strong stratification approximation on describing large-amplitude internal solitary waves with pycnocline, this paper uses the two- and three-layer MCC internal wave models to calculate the wave profile and wave speed of large-amplitude internal solitary waves and compares them with the DJL equation, which considers continuous density stratification. The conclusions are as follows.

1) When pycnocline thickness is small ($d/H = 3\%$), the results of the two- and three-layer MCC internal wave models and the DJL equation are in good agreement with the experimental values, indicating that introducing the strong stratification approximation does not lead to significant errors.

2) When the pycnocline thickness is relatively large ($d/H = 8\%$ or 10%), significant differences between the results of the two-layer MCC internal wave model and the DJL equation are observed. Wider wave profiles and larger wave speeds are obtained by the two-layer MCC internal wave model compared with those obtained by the DJL equation. When the pycnocline thickness increases from

8% to 10%, the error introduced by the two-layer approximation becomes larger. In contrast, the three-layer MCC internal wave model remains in good agreement with the DJL equation regarding wave profile and wave speed. As demonstrated, although the pycnocline thickness is large, the error introduced by the three-layer approximation, rather than the two-layer approximation, remains small in the section considered here but should be noted in general.

Funding Supported by the Fundamental Research Funds for the Central Universities (No. 3072022FSC0101), the National Natural Science Foundation of China (Nos. 12202114, 52261135547), the China Postdoctoral Science Foundation (No. 2022M710932), the State Key Laboratory of Coastal and Offshore Engineering, Dalian University of Technology (No. LP2202), the Qingdao Postdoctoral Application Project, and the Heilongjiang Touyan Innovation Team Program.

References

- Barros R, Choi W, Milewski PA (2020) Strongly nonlinear effects on internal solitary waves in three-layer flows. *Journal of Fluid Mechanics* 883: A16. <https://doi.org/10.1017/jfm.2019.795>
- Camassa R, Choi W, Michallet H, Rusås PO, Sveen JK (2006) On the realm of validity of strongly nonlinear asymptotic approximations for internal waves. *Journal of Fluid Mechanics* 549: 1-23. <https://doi.org/10.1017/S0022112005007226>
- Camassa R, Tiron R (2011) Optimal two-layer approximation for continuous density stratification. *Journal of Fluid Mechanics* 669: 32-54. DOI: 10.1017/S0022112010004891
- Cheng MH, Hsu JRC (2014) Effects of varying pycnocline thickness on interfacial wave generation and propagation. *Ocean Engineering* 88: 34-45. <https://doi.org/10.1016/j.oceaneng.2014.05.018>
- Choi W, Camassa R (1999) Fully nonlinear internal waves in a two-fluid system. *Journal of Fluid Mechanics* 396: 1-36. <https://doi.org/10.1017/S0022112099005820>
- Cui J, Dong S, Wang Z (2021) Study on applicability of internal solitary wave theories by theoretical and numerical method. *Applied Ocean Research* 111: 102629. <https://doi.org/10.1016/j.apor.2021.102629>
- Du H, Wei G, Wang SD, Wang XL (2019) Experimental study of elevation- and depression-type internal solitary waves generated by gravity collapse. *Physics of Fluids* 31(10): 102104. <https://doi.org/10.1063/1.5121556>
- Dubreil-Jacotin ML (1934) Sur la détermination rigoureuse des ondes permanentes périodiques d'amplitude finie. *Journal de Mathématiques Pures et Appliquées* 13: 217-291
- Dunphy M, Subich C, Stastna M (2011) Spectral methods for internal waves: Indistinguishable density profiles and double-humped solitary waves. *Nonlinear Processes in Geophysics* 18(3): 351-358. <https://doi.org/10.5194/npg-18-351-2011>
- Gao YX, You YX, Wang X, Li W (2012) Numerical simulation for the internal solitary wave based on MCC theory. *Ocean Engineering* 30(4): 29-36. <https://doi.org/10.16483/j.jissn.1005-9865.2012.04.014>
- Gong Y, Xie J, Xu J, Chen Z, He Y (2022) Oceanic internal solitary waves at the Indonesian submarine wreckage site. *Acta Oceanologica Sinica* 41(3): 109-113. <https://doi.org/10.1007/s13131-021-1893-0>
- Grue J, Jensen A, Rusås PO, Sveen JK (1999) Properties of large-amplitude internal waves. *Journal of Fluid Mechanics* 380: 257-278. <https://doi.org/10.1017/S0022112098003528>
- Huang WH, You YX, Wang X, Hu TQ (2013) Wave-making experiments and theoretical models for internal solitary waves in a two-layer fluid of finite depth. *Acta Physica Sinica* 62(8): 786-790. <https://doi.org/10.7498/aps.62.084705>
- Huang X, Chen Z, Zhao W, Zhang Z, Zhou C, Yang Q, Tian J (2016) An extreme internal solitary wave event observed in the northern South China Sea. *Scientific Reports* 6(1): 1-10. <https://doi.org/10.1038/srep30041>
- Jo TC, Choi YK (2014) Dynamics of strongly nonlinear internal long waves in a three-layer fluid system. *Ocean Science Journal* 49(4): 357-366. <https://doi.org/10.1007/s12601-014-0033-6>
- Koop CG, Butler G (1981) An investigation of internal solitary waves in a two-fluid system. *Journal of Fluid Mechanics* 112: 225-251. DOI: 10.1017/S0022112081000372
- Kuang GR (1986) The analysis of density and spring layer. *Shan Dong Hai Yang Xue Bao* (S1): 60-73, 129. DOI: 10.16441/j.cnki.hdxh.1986.s1.006. (in Chinese)
- la Forgia G, Sciortino G (2019) The role of the free surface on interfacial solitary waves. *Physics of Fluids* 31(10): 106601. <https://doi.org/10.1063/1.5120621>
- la Forgia G, Sciortino G (2021) Free-surface effects induced by internal solitons forced by shearing currents. *Physics of Fluids* 33(7): 072102. <https://doi.org/10.1063/5.0055466>
- Long RR (1953) Some aspects of the flow of stratified fluids: I. A theoretical investigation. *Tellus* 5(1): 42-58. <https://doi.org/10.3402/tellusa.v5i1.8563>
- Lu H, Liu Y, Chen X, Zha G, Cai S (2021) Effects of westward shoaling pycnocline on characteristics and energetics of internal solitary wave in the Luzon Strait by numerical simulations. *Acta Oceanologica Sinica* 40(5): 20-29. <https://doi.org/10.1007/s13131-021-1808-0>
- Miyata M (1985) An internal solitary wave of large amplitude. *La Mer* 23(2): 43-48
- Miyata M (1988) Long internal waves of large amplitude. Horikawa, K., Maruo, H. (eds) *Nonlinear Water Waves*. International Union of Theoretical and Applied Mechanics. Springer, Berlin, Heidelberg. https://doi.org/10.1007/978-3-642-83331-1_44
- Stastna M, Lamb KG (2002) Large fully nonlinear internal solitary waves: The effect of background current. *Physics of Fluids* 14(9): 2987. <https://doi.org/10.1063/1.1496510>
- Stastna M, Lamb KG (2020) An interesting oddity in the theory of large amplitude internal solitary waves. *Russian Journal of Earth Sciences* 20(4): 5
- Wang Z (2021) On the properties of ocean solitary waves with and without currents. PhD thesis, Harbin Engineering University, Harbin, 95-96
- Xie J, Jian Y, Yang L (2010) Strongly nonlinear internal soliton load on a small vertical circular cylinder in two-layer fluids. *Applied Mathematical Modelling* 34(8): 2089-2101. <https://doi.org/10.1016/j.apm.2009.10.021>
- Zhang TY, Wang Z, Wang ZH, Xie BT, Zhao BB, Duan WY, Hayatdavoodi M (2020) On mode-1 and mode-2 internal solitary waves in a three-layer fluid system. *Proceedings of the 35th International Workshop on Water Waves and Floating Bodies (IWWWFB)*, 173-176
- Zou L, Ma XY, Li ZH (2020) Experimental reconstruction and flow-field analysis of stratified fluid soliton model. *Journal of Harbin Engineering University* 41(2): 263-270. DOI: 10.11990/jheu.201905113